ACS Catalysis

Research Article

pubs.acs.org/acscatalysis

Adsorption and Activation of Ethene in Transition Metal Exchanged Zeolite Clinoptilolite: a Density Functional Study

Ellie L. Uzunova*[,†] and Hans Mikosch[‡]

[†]Institute of General and Inorganic Chemistry, Bulgarian Academy of Sciences, Sofia 1113, Bulgaria,

[‡]Institute for Chemical Technologies and Analytics, Vienna University of Technology, Getreidemarkt 9/E164-EC, 1060 Vienna, Austria

Supporting Information

ABSTRACT: Ethene adsorption in transition-metal-exchanged clinoptilolite with cations of the d elements (Fe−Cu) and also Pd was examined by density functional theory with the B3LYP functional, using the embedded cluster method in ONIOM. The preferred extraframework cation sites for the divalent cations are those in the large channel A. The monovalent cations Ni^+ and Cu^+ show little preference toward the available cation sites: they approach a center of negative framework charge, forming shorter M−O bonds as compared with the divalent cations. Periodic model calculations were applied to validate the extraframework site preference of Cu^+ cations, and they confirm the ONIOM results, though periodic calculations systematically predict smaller energy gaps between the different cation site occupancies. A dominant component in the formation of the metal cation−adsorbate π-complexes is the electron charge transfer from the filled d orbitals of the transition metal cations to the unoccupied π^* orbitals of ethene. Significant contribution of the framework oxygen atoms as electron donors to the cations was revealed. This results in lengthening of the C═C bond and a red shift of the corresponding stretching vibration, which is most pronounced in the adsorption complexes with monovalent cations, (Ni^+, Cu^+, Pd^+). The hydrogen atoms in the ethene molecule become nonequivalent upon adsorption. The C−H bond lengthening is more significant for the adsorption complexes in channel B and on Ni^+ cations in channel A. The deformation density maps, derived from the B3LYP calculated densities provide insight into the role of the framework in the charge transfer from the metal cations to the ethene molecule.

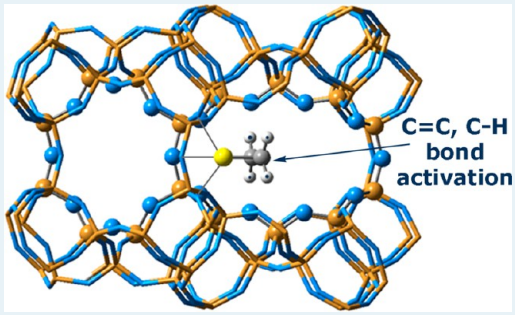

KEYWORDS: *electronic structure, density functional calculations, natural zeolite, ONIOM, clinoptilolite, ethene adsorption*

INTRODUCTION

Zeolites find a broad number of applications as a result of their unique opened framework architecture and the presence of regularly spaced cavities and channels, which are intrinsic properties of the structure.[1] The framework of zeolites and zeolite-like microporous materials (for example, galosilicates and aluminophosphates) is built by corner-sharing tetrahedra TO_4, in which the tetrahedral atom is Si, Al, P, Ga, etc.; each oxygen atom bridges adjacent tetrahedra, and this presumes a ratio of O/T = 2. The windows that open to the pore system have dimensions comparable to those of small molecules; thus, zeolites are able to discriminate molecules on the basis of their size and act as "molecular sieves". The zeolite framework is negatively charged because of Al → Si substitution at tetrahedral sites, and this charge is compensated by either a proton to form bridging hydroxyl groups, −Al−OH−Si−, or by an extraframework cation. Many separation processes rely on zeolites, and they are also employed as ion-exchangers, adsorbents, and catalysts.[1,2]

Adsorption of the reactants is the key process for both separation and catalysis, and this is the main topic of theoretical and experimental studies that target the design of new zeolite materials or modification of the available ones. Small molecules—CO, NO, NO_2, ethene, ethyne—are usually used as adsorbates to probe an active site, and the applied experimental techniques involve XRD, temperature-programmed desorption, IR spectroscopy and microcalorimetry.[3−11] Zeolites in H-form (with protons as charge counterpart) act as solid acids and catalyze a number of reactions in petrochemistry.

The indispensable role of transition metal cation exchanged zeolites was revealed for redox catalytic reactions, for example, the selective reduction of nitrogen oxides, NO_x, with hydrocarbons.[5] The role of transition metal centers, their preferred location, and the reaction mechanism became a challenge for theoretical studies.[11−14] Ag^+- and Cu^+-exchanged zeolites were studied in relation to olefin−paraffin separation by π-complexation, and the first members of the series, ethene and ethane, became useful also as probe molecules for testing the electron-donor properties of different transition metal cations.[11,12] The activation of C═C, C≡C, and C═O bonds in Cu^+- and Ag^+-exchanged ZSM-5 was examined by the

Received: July 24, 2013
Revised: September 30, 2013
Published: October 15, 2013

   dx.doi.org/10.1021/cs4005997 | ACS Catal. 2013, 3, 2759−2767

embedded cluster approach, and the diversification of the two cations by the zeolite environment was outlined.[14b,c] Experimental studies of a fully exchanged Ag^+−X zeolite found that ethene was reduced to form carbanions $C_2H_2^{2-}$, and the role of Ag^0, together with the presence of lattice oxygen vacancies, was revealed.[6d] Ni(II)- and Pd(II)-exchanged zeolites, including synthetic clinoptilolite, were examined in ethene dimerization.[15,16] The reduced Ni^+ cations formed the active site, but the presence of alkali cations boosted the activity.

Natural zeolites, however, find applications as ion-exchangers and adsorbents rather than catalysts.[17] The clinoptilolite mineral, for example, contains admixtures of mordenite, iron oxides, and quartz;[20] therefore, synthetic analogs with the same topology (e.g. LZ-219, CIT-3) are preferred for reliable testing as catalysts.[16,18] Structural studies by X-ray diffraction on the location of extraframework transition metal and heavy metal cations in natural clinoptilolite were limited to the hydrated forms; thus, for small cations, such as Cu^{2+}, linkages to framework oxygen atoms were not reported, and they were detected in the center of the large A channel of clinoptilolite, coordinated by water molecules only.[19] The size of channel A proved to be large enough to host the tetramonia complex $[Cu(NH_3)_4]^{2+}$, coordinated further to two water molecules.[44] Ni^+ cations, obtained after reduction of Ni(II)-exchanged clinoptilolite, were examined by electron spin resonance (ESR) and electron spin echo modulation (ESEM), which revealed two sites that these cations occupy.[16a,c] The good performance of Ni-clinoptilolite in ethane dimerization to *n*-butenes[16] challenged theoretical studies, as well, but the large size of the unit cell limited the models to relatively small size.[13] The divalent cations of the 3d elements preferred coordination to five-member rings in ZSM-5, according to DFT studies using cluster models,[4a] whereas for the divalent cations of the noble metals, the sites in six-member rings were found more favorable. In clinoptilolite, the cations find positions in larger rings, and they are more exposed to the inner part of the channels; therefore, cluster models are not applicable.

In the present study, transition-cation-exchanged clinoptilolite with Fe^{2+}, Co^{2+}, Ni^{2+}, Ni^+, Cu^{2+}, Cu^+, Pd^{2+}, and Pd^+ at extraframework cation sites is described by density functional theory by applying the embedded cluster method in ONIOM and using the B3LYP functional. The elements from the second half of the first transition row were selected because their divalent cations possess partly filled d orbitals, d^6−d^9, and the π-coordination to ethene is expected to be strengthened by a strong metal-to-ligand charge transfer component. Pd was selected among the noble metals because in the divalent state, a $4d^8$ configuration is formally adopted, and it would be interesting to trace the differences to Ni(II) $3d^8$. The preferred locations of cations among the different extraframework cation sites in the dehydrated zeolite are evaluated on the basis of the relative energies of the optimized embedded cluster models in ONIOM. The binding energies of ethene, adsorbed at different cations, are calculated, and the IR and Raman frequencies and frequency shifts upon adsorption are estimated. Periodic boundary conditions (PBC) were applied to Cu^+-exchanged clinoptilolite, and the structural changes have been compared with alkali and alkaline-earth-cation-containing clinoptilolite, for which detailed experimental data are available.

STRUCTURE AND METHODS

Clinoptilolite is the subject of numerous studies because it is available as a natural zeolite in large deposits worldwide. It has the same topology as the mineral Heulandite and, thus, belongs to the same structural group, denoted as HEU.[22] The structure is a very open one and possesses a 2D net of intersecting channels in the [010] plane, with three main channels: A, accessible via 10-member rings of size 3.1 × 7.5 Å; B, accessible via symmetric 8-member rings of size 3.6 × 4.6 Å; and C, accessible via 8-member-rings of size 2.8 × 4.7 Å, the latter belonging to the side-wall between channels A and B. Channels A and B run in the direction to the *c*-axis, whereas channel C intersects both channels A and B and is parallel to the *a*-axis (see Figure 1). The framework density of clinoptilolite is quite

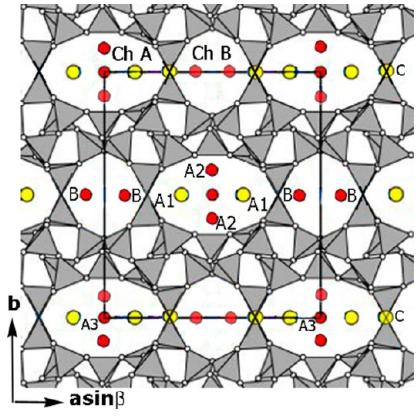

Figure 1. The clinoptilolite structure viewed along the c vector with the main channels A and B and the available extraframework cation sites. A1, A2, and A3 lie in channel A; B sites are positioned in channel B; C sites lie in channel C and are located inside the 8-member rings, which open into the A and B channels. The notation of cation sites of ref 19 is used; A1, B, and C correspond to M1, M2, and M3 in the notation of Koyama and Takéuchi, ref 24.

low, 17.7 T/1000 $Å^3$, and is comparable to that of pentasil zeolites with MFI topology. The extraframework cation sites have been determined in early crystallographic studies of mineral samples and were summarized by Alberti[23] and Koyama et al.[24] for alkali and alkaline-earth cations. Additional sites in the A channels were reported for heavy-metal cations such as Cd^{2+} and Pb^{2+}.[19]

Following the notation of Godelitsas et al.,[19] three distinct cation sites are available in channel A to transition metal cations: A1, A2, and A3 (see Figure 2). In channel B, there is one site, located in proximity to the T2−O−T2 bridges, denoted as B site. In channel C, which is an intersecting channel, we find the C site, located inside the eight-member rings, displayed in Figure 1. The site A3 in the center of channel A was found to be occupied by water-molecule-coordinated small-size cations, such as Mg^{2+}, Cu^{2+}, which had no contacts with the framework oxygen atoms.[19] It is unlikely that this site could be occupied by extraframework cations in dehydrated clinoptilolite because it does not provide optimal coordination by framework oxygen atoms, but at elevated temperatures of 300 °C, part of the Na^+ cations migrated to site A3.[39] Sites in the channel center, when available to extraframework cations in zeolites, cannot be expected to form a stable adsorption site.[21]

The periodic calculations were performed with Gaussian 09 using the PBE density functional; the Brillouin-zone sampling was restricted to the Γ point.[27,28] The unit cell consists of 108 framework atoms, and ratios of Si/Al in the range 6.0−9.0 were examined. All electrons, including core ones, were explicitly included in the periodic DFT calculations. In studies of

dx.doi.org/10.1021/cs4005997 | ACS Catal. 2013, 3, 2759−2767

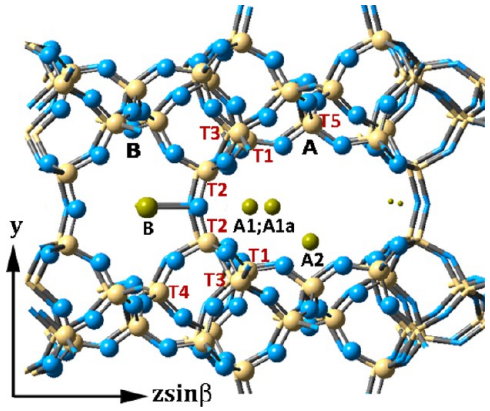

Figure 2. The clinoptilolite structure viewed along the *x*-axis with the main channels A and B and the extraframework cation sites, occupied by transition metal cations in the dehydrated zeolite. Oxygen atoms are blue, Si are light brown, and extraframework cations are light green. Tetrahedral atom numbers according to ref 24 are indicated.

polysiloxanes, the importance of applying polarization functions for T-atoms (Si, Al), rather than for oxygen, has been stressed;[29] therefore, we have used the standard 3-21G* basis set for the framework atoms with added polarization functions for the second row elements (Si, Al). The 6-31G(d) basis was used for Na^+, K^+, and Ca^{2+}, and the 6-311G(d) basis set was used for the copper cations.

A two-layer model was adopted for the ONIOM calculations, QM/MM, as implemented in Gaussian 09.[25−27] The high layer was assessed by the B3LYP hybrid density functional[30−32] using the 6-31G(d,p) basis set for framework atoms, carbon, and hydrogen; the 6-311G(d) basis set was applied to transition metal cations of the 3d elements.[33] For the Pd^{2+} and Pd^+ cations, the split-valence QZVP basis set and the corresponding pseudopotential for the core electrons were applied.[34,35] The universal force field (UFF) was used for describing the low layer, and no atoms were constrained except the most outer ones, which terminate the whole system; they were pinned at the crystallographic positions to avoid optimization to non-zeolitic species.[26,36] The electrostatic interactions between the "high" and "low" layers were not considered, that is, the calculations were performed using "mechanical embedding" but not "electronic embedding." The periodic model calculations for the coordination of Cu^+ cations in the A and B channels agree very well with the ONIOM results. Previous ONIOM studies on zeolites,[26,38c] have proved that calculating energy differences between similar framework configurations, such as proton (extraframework cation) site preference or a reaction barrier, cancels the effect of long-range slowly varying interactions and leaves reaction energies controlled only by local electronic interactions.

UFF is a generic nonreactive force field that contains parameters for all elements of the periodic table and is thus applicable for the elements included in the present study, although the parametrization for silicates lacks partial charges. The low level thus includes minimal electronic effects and is close to a ball-and-spring model, which allows us to take into account the framework constraint only, ignoring long-range forces. This is justified for our system with high Si/Al ratio and small number of extraframework atoms per unit cell: 4−7 extraframework cations per 108 framework atoms in the unit cell with general formula $(M^{n+})_{x/n}Si_{36-x}Al_xO_{72}$. Moreover, the Dempsey's rule implies maximum separation between the framework negative charges and the cations also follows this rule, as they form ion pairs with the nearest framework Al → Si substitution. The "high" layers are sufficiently large and represent the interactions of the adsorption centers, the adsorbed ethene molecules with the framework oxygen atoms at the QM level of theory.

Geometry optimizations were performed using the "quadratic macro coupling" method,[26] which couples forces between the QM and MM layers in a numerically stable manner to produce more accurate steps in optimization. Si/Al ratios in the range 4.5−9.0 were examined, and ONIOM models of different sizes were tested. The largest one consisted of 16T/100T atoms, and they were used to calculate the cation site preferences. The high layer in these models consisted of the neighboring 8-member ring of channels B and C and the 10-member ring of channel A, as shown in Figure 3a. Al → Si substitution in the low layer was also applied to maintain the

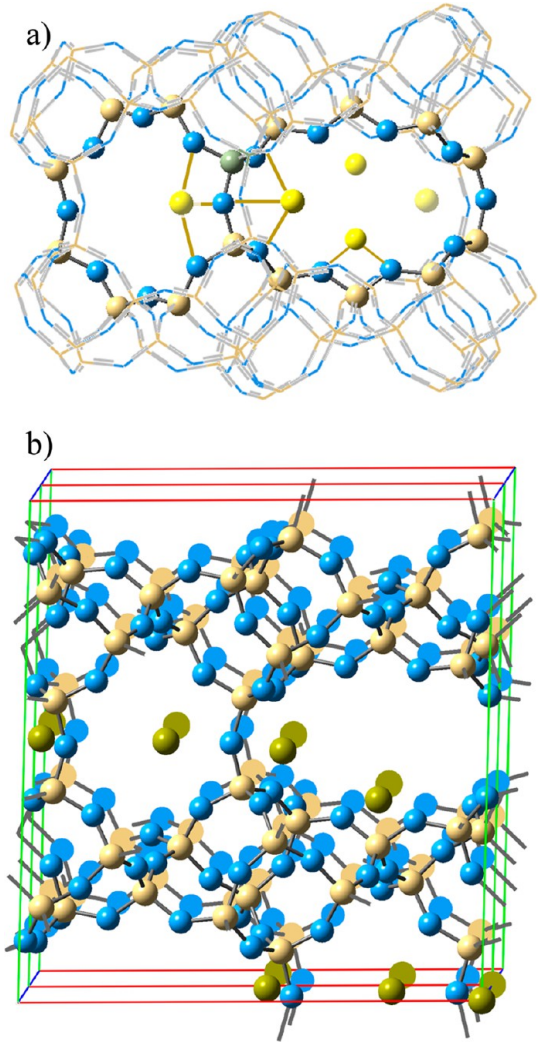

Figure 3. Structural models used in optimization. (a) The 16T/100T ONIOM models with the main cation sites. The low layer, described by molecular mechanics (MM) is shown as wireframe. (b) The unit cell of clinoptilolite, replicated along the c vector. The main cell is represented by sticks and balls; the atoms of the replicated cell are shown as disks. The replication along "c" gives an idea of the close appearance of cations in periodic studies of unit cells with a small value of the *c* parameter.

dx.doi.org/10.1021/cs4005997 | ACS Catal. 2013, 3, 2759−2767

Si/Al ratio, and the Al positioning at T-sites obeyed Löwenstein's rule for avoidance of Al−O−Al linkages and Dempsey's rule for maximum separation of negative framework charges. Smaller sized 10T/76T models proved sufficient to describe cation sites A1 and A2 and the adsorption of ethene in channel A.

Frequency calculations were performed for the finite models to justify the optimized configurations as points of energy minima; ethene vibrations were evaluated, and corrections for anharmonicity were applied.[37] The total electron density and the electrostatic potential (ESP) of the clusters were calculated from the B3LYP density. Molecular electrostatic potential (MEP) and deformation density maps in which the effects of metal-to-ligand charge transfer can be detected and areas of enhanced reactivity in the zeolite structure can be discerned were derived.

CATION SITE PREFERENCE OF DIVALENT CATIONS OF THE D ELEMENTS (FE−CU); MONOVALENT CU(I) AND NI(I), AND PD(II) IN CLINOPTILOLITE

The periodic model calculations with Ca^{2+}-, Na^{+}-, K^{+}-, and Cu^{+}-exchanged clinoptilolite indicate that the transition metal cation causes only local deformation at the site, where it resides, evidenced by singular lengthened Si−O and Al−O bonds, whereas the presence of Ca^{2+} cations causes broadening of the T1−O−T2 angles (see Table 1 and Figure 2). The unit cell parameters calculated for Ca- and Na-containing clinoptilolite agree with experimental data; Cu^{+} exchange leads to minor shrinking of the cell along the [100] and [010] directions, compared with Na^{+}-exchanged clinoptilolite. The *c* parameter, however, is slightly increased, indicating distortion of the C rings. Both Na^{+} and Cu^{+} prefer positions in the vicinity of T2−O−T2 linkages, either in channel A or in channel B. The Cu^{+} cations form shorter bonds to the framework oxygen atoms than the Na^{+} cations, and both the A1 and B sites are coordinated to oxygen atoms from the side C rings, which interconnect channels A and B. Similar results about nonuniform local deformations are obtained by ONIOM, and they are not larger compared with other frameworks, such as FAU and CHA, for which cluster, periodic, and ONIOM calculations were performed,[38a−c] as well as for alkali- and alkaline-earth-cation-exchanged clinoptilolite.[38d]

ONIOM and PBC calculations predict correctly the coordination of cations to framework oxygen atoms, and the calculated internuclear distances do not differ significantly. However, the relative energies for the different cation sites are smaller at the PBC level. The Cu^{+} cations interact more strongly with the framework than the alkali cations K^{+} and Na^{+}, although the coordination number of the monovalent cations to the oxygen atoms is, in most cases, equal to 2. Cu^{+} is able to reach coordination by three framework oxygen atoms at sites A1, forming two shorter and one longer Cu−O bonds (see Table 1). ONIOM predicts the A1 site as more stable than the A2 and B sites for Cu^{+} cations by 26.2 and 35.1 kJ mol^{-1}, respectively (see Table 2), whereas PBC predicts much smaller energy gaps of 16.7 and 21.1 kJ mol^{-1}.

Table 1. Unit Cell Parameters, Bond Lengths (Å), and Bond Angles (∠TOT, deg) in Cation-Exchanged Clinoptilolite, As Calculated by Periodic Models Using the PBE Density Functional

cation, site	Ca^{2+} (A1)	Na^{+} (A1)	K^{+} (C)	Cu^{+} (A1)	Cu^{+} (B)
M−O_z[a]	2.351, 2.380, 2.384, 2.398	2.233, 2.423	2.767, 2.794	1.937, 1.966, 2.391	1.889, 1.946
Si(T2)−O	1.672	1.675	1.621	1.639	1.645
Al(T2)−O	1.769	1.763	1.757	1.770	1.783
Si(T3)−O	1.663	1.653	1.673	1.629	1.623
Al(T3)−O	1.789	1.772	1.769	1.783	1.765
Si(T1)−O	1.669	1.656	1.667	1.644	1.632
Al(T1)−O	1.791	1.773	1.771	1.790	1.754
T2−O−T2	148.1	147.2	152.1	147.4	152.3
T2−O−T3	145.2	140.5	147.3	156.2	159.7
T2−O−T1	161.9	135.2	131.2	133.9	145.3
unit cell	a = 17.612 Å, b = 17.837 Å, c = 7.416 Å, α = 88.1°, β = 113.5°, γ = 90.5° (Ca^{2+})				
	a = 17.674 Å, b = 17.961 Å, c = 7.417 Å, α = 87.9°, β = 113.9°, γ = 89.7° (Na^{+})				
	a = 17.781 Å, b = 18.154 Å, c = 7.430 Å, α = 89.7°, β = 114.3°, γ = 90.0° (K^{+})				
	a = 17.632 Å, b = 17.959 Å, c = 7.471 Å, α = 90.1°, β = 114.3°, γ = 90.5° (Cu^{+})				
exptl[b]	a = 17.660 Å, b = 17.963 Å, c = 7.400 Å, α = 90°, β = 116.47°, γ = 90.0° (Ca^{2+})				
	a = 17.4030(10) Å, b = 18.0120(10) Å, c = 7.4350(10) Å, α = 90.0°, β = 113.812(2)°, γ = 90.0° (Na^{+})				
	a = 17.688(16) Å, b = 17.902(9) Å, c = 7.409(7) Å, α = 90°, β = 116.50(7)°, γ = 90.0° (K^{+})				

[a]Cation to nearest framework oxygen atom internuclear distances. [b]Experimental unit cell parameters are from refs 24, 39, and 41.

Table 2. Relative Energies (kJ mol^{-1})[a] of Configurations with Cations at Different Extraframework Cation Sites in the Main Channels of Clinoptilolite,[b] Calculated by ONIOM

cation	state	channel A, site A1	channel A, site A1a	channel A, site A2	channel B, site B	channel C, 8-member rings
Fe^{2+}	^{5}A	10.5	0.0		30.3	165.4
Co^{2+}	^{4}A	12.4	0.0		40.6	145.4
Ni^{2+}	^{3}A	9.7	0.0		75.5	131.2
Ni^{+}	^{2}A	16.0		0.0	24.4	137.2
Cu^{2+}	^{2}A	0.0			68.1	90.4
Cu^{+}	^{1}A	0.0		26.2	35.1	59.0
Pd^{2+}	^{1}A		0.0		46.6	79.8
Pd^{+}	^{2}A		0.0		69.7	

[a]The relative energies are calculated as differences from the ONIOM energy of the ground state configurations for the exchanged extraframework cations. [b]The coordination of cations in channels A and B is shown in the Supporting Information.

Periodic boundary conditions can be applied to reliably describe the framework properties, but the extraframework cation sites, which have partial occupancies, as well as the active sites for adsorption and catalysis, do not follow the periodicity of the unit cell (see Figure 3b). For zeolites with small unit cells, it is applicable to include more than one cell explicitly in the calculations to describe in a more realistic way the randomly occupied cation sites. The unit cell of clinoptilolite is a relatively large one, but the "*c*" unit cell parameter is about half the size of the "*a*" and "*b*" parameters and compares with the size of the windows. Similarly, for mordenite, *c*/*a* and *c*/*b* ratios are even smaller.[22] Cation sites, studied with periodic models, would appear in artificial ordering and at close distances along the [001] direction in mordenite and heulandite/clinoptilolite frameworks. Cluster models, and

dx.doi.org/10.1021/cs4005997 | ACS Catal. 2013, 3, 2759−2767

embedded cluster models are thus able to provide a more accurate representation of the framework and the extraframework cations for which different locations can be examined without artificial repetition in space.[4,13,14,26c,38] The computational time required for ONIOM calculations is also more reasonable and allows the use of hybrid density functionals (B3LYP), which provides accurate results for the band gaps in insulator materials, such as aluminosilicates, their ordering by stability of different cation sites in zeolites, the activation energies, and the vibrational frequencies of adsorbed species.[4,26c]

Among the three distinct extraframework cation positions available in channel A and one in channel B, transition metal cations occupy those that are close to the framework oxygen atoms; thus, no occupancy of the A3 site was found. The sites in channel A are preferred to those in channel B, and the sites C, in the eight-member rings of the C channel, are the least favorable (see Table 2). Sites C are unlikely to be occupied by divalent cations because the energy required to accommodate them in the rings is significant, and deformation of the rings occurs so as to provide optimal coordination. A trend of decrease by energy for the divalent cations from Fe to Ni is found for positions B and C, which indicates that the larger cations, Fe^{2+} and Co^{2+}, would prefer to reside in the large channel. For the smaller cations, Ni^{2+}, Cu^{2+}, and Pd^{2+}, higher occupancies of site B can be expected, although the A channel sites would still be preferred.

Fe^{2+} is in quintet ground state, and the calculated energy required for excitation to the triplet state is 1.0 eV at the B3LYP level of theory, compared with 0.73 eV by applying the PBE density functional. Co^{2+} is in the quartet ground state, which is 0.69 eV below the doublet state, as calculated by B3LYP; the PBE calculated value is 0.54 eV. For the cation of the next d element, Ni^{2+}, the energy between the triplet ground state and the singlet state is higher, 1.1 eV, according to the B3LYP calculations, and 0.79 eV indicated by PBE. Although PBE predicts systematically smaller energy differences, there is no discrepancy between the ground states of the cations, and the energy separations between the spin states remained unchanged (within 0.04 eV) in the adsorption complexes.

Strong electrostatic potential is induced in the main channels of clinoptilolite by the oxygen atoms that belong to the large rings (8- and 10-member rings), and divalent cations at sites B do not quench the nucleophilic properties. Broad nucleophilic areas, which indicate several maxima, develop in both channels A and B (see Figure 4). This allows splitting of the A1 site into two closely spaced sites, A1 and A1a, which was found for Fe^{2+}, Co^{2+}, and Ni^{2+}. Site A1a approaches the center of the 10-member ring, and site A1 provides more favorable coordination to the side-wall atoms. Al → Si substitution at the tetrahedral site T1 favors the A1a site; however, the energy gaps are rather small, within 9.7−12.4 kJ mol^{-1}, so an averaged structure can be predicted at elevated temperature. The monovalent cations Ni^{+} and Cu^{+} are coordinated by only two framework oxygen atoms at sites A2 and B (see Table 3). The same applies to monovalent Pd^{+} cations, but the larger cation size in this case implies longer Pd^{+}−O bonds and a preference toward the A1a site in the large channel. Copper cations, either divalent or monovalent, do not find optimal coordination in the clinoptilolite framework and they show little preference between sites B and C. Neither does the A2 site provide favorable coordination to Cu^{+}, whereas it is preferred by Ni^{+}, a result that indicates the selectivity of extraframework cation sites in clinoptilolite toward small-size cations. It can be expected that upon reduction of Ni^{2+} cations to Ni^{+}, they would easily migrate from the A1a sites to the A2 sites.

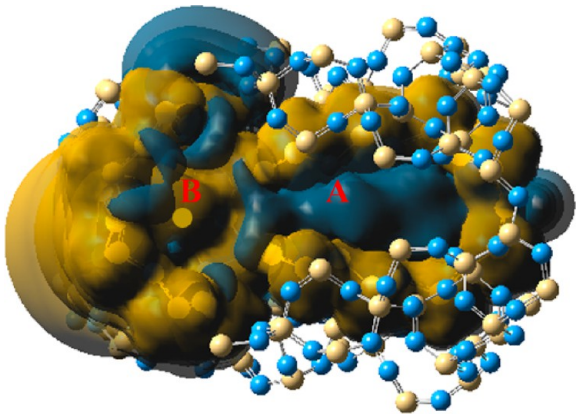

Figure 4. The molecular electrostatic potential (MEP) map inside channels A and B of clinoptilolite with Ca^{2+} at site B. Channels A and B are denoted (red). Areas of positive EP (electrophilic) are yellow; the negative EP (nucleophilic) are displayed in blue.

■ ETHENE ADSORPTION AT TRANSITION METAL CATION CENTERS IN CLINOPTILOLITE

The IR spectrum of ethene in the gas phase contains bands originating from the C−H vibrations in the high-frequency region (see Table 4). The C═C stretching vibration at 1623 cm^{-1} is sensitive to the formation of π-complexes with transition metal cations, and it is only Raman-active. The B3LYP calculated anharmonic vibrational frequencies of ethene match the experimental data with the exception of the C═C vibration, which is overestimated by 60 cm^{-1}. Ethene always binds symmetrically to transition metal cations and forms metal−carbon bonds with both carbon atoms. The cations of the elements from the second half of the row and also the cations of Pd have a nearly filled outer d-electron shell (or completely filled in the case of Cu^{+}), and the electron charge transfer from the metal cation to the unfilled π^* orbitals of ethene is a dominant component in the formation of the adsorption complex. To what extent this occurs can be estimated by the lengthening of the C═C bond and the red shift of the C═C stretching vibration in the spectra.

The ethene molecule has a free diameter of 4.2 Å, and it can diffuse along all clinoptilolite channels, but channel A would provide the best path, as the presence of cations on one side of the 10-member ring window would not block the entrances. Upon adsorption at transition metal cation centers, the ethene molecule loses its D_{2h} symmetry. The change in geometry of adsorbed ethene involves not only the C═C bond, the hydrogen atoms also experience the effect of metal-to-ligand charge transfer and the strong electrostatic field in the zeolite cavity. The C−H bonds undergo minor lengthening/shortening, which varies among the bonds. As a result, all vibrational modes of ethene become IR-active, and splitting of the C−H vibrations is also observed.

IR spectroscopy has been extensively used for studying olefin adsorption in zeolites.[4,7−9] The divalent cations are coordinated to three framework oxygen atoms prior to adsorption, and this applies to both A1 and B sites (see Table 3 and Supporting Information). At B sites, the three M−O bonds have more uniform bond lengths, and for the small-sized divalent cations

dx.doi.org/10.1021/cs4005997 | ACS Catal. 2013, 3, 2759−2767

Table 3. Internuclear Distances between Extraframework Cations and Nearest Zeolite Framework Oxygen Atoms (O_z) before Adsorption, $R_{M-O(z)}$; and with an Adsorbed Ethylene Molecule, $R_{M-O(z)\ ads}$; Carbon−Carbon Bond Length, $R_{C=C}$; Carbon−Hydrogen Bond Length, R_{C-H}; Cation−Carbon Internuclear Distances, R_{M-C}; Adsorption Energies; and IR active Vibrational Frequencies, υ, of the C_2H_4 Molecule Adsorbed

cations/ site	$R_{M-O(z)}$, Å	$R_{M-O(z)\ ads}$, Å	$R_{C=C}$, Å/ $\Delta R_{C=C}$,[a] Å	R_{C-H}, Å	R_{M-C}, Å	E_{ads}, kJ mol^{-1}	υ, cm^{-1}
Channel A							
Fe^{2+} (A1a)	1.961, 1.995, 2.215	1.954, 1.964, 2.745	1.366/0.036	1.085−1.086	2.235, 2.277	79.5	1400, 1543, 3007, 3113, 3137
Co^{2+} (A1a)	1.939, 1.960, 2.320	1.920, 1.922, 2.814	1.360/0.030	1.088−1.090	2.222, 2.250	82.9	1444, 1592, 2993, 3177, 3198
Ni^{2+} (A1a)	1.922, 1.953, 2.281	1.928, 1.929, 2.154	1.356/0.026	1.086−1.088	2.259, 2.296	69.9	1401, 1589, 2999, 3103, 3131
Ni^{+} (A1)	1.931, 2.035, 2.155	2.008, 2.365, 2.391	1.385/0.055	1.083−1.086	2.021, 2.053	140.1	1400, 1528, 3005, 3102, 3135
Ni^{+} (A2)	1.930, 1.957	2.009, 2.017	1.399/0.069	1.085−1.091	1.970, 1.971	196.4	1445, 1535, 2969, 3005, 3048, 3097
Cu^{2+} (A1)	1.903, 1.907, 2.676	1.919, 1.927, 2.167	1.364/0.034	1.084−1.086	2.243, 2.276	90.9	1400, 1551, 3041, 3122, 3158
Cu^{+} (A1)	1.913, 1.997, 2.429	1.977, 2.021	1.391/0.061	1.087−1.089	1.959, 1.965	223.2	1443, 1544, 2987, 3071, 3092
Cu^{+} (A2)	1.950, 1.972	1.995, 2.037	1.391/0.061	1.087−1.089	1.962, 1.965	241.2	1444, 1546, 2986, 3069, 3093
Pd^{2+} (A1a)	2.031, 2.042, 2.271	2.133, 2.147, 2.232	1.385/0.055	1.083−1.087	2.164, 2.178	136.9	1431, 1544, 3024, 3121, 3140
Pd^{+} (A1a)	2.157, 2.242	2.164, 2.273	1.379/0.049	1.085−1.088	2.194, 2.200	129.0	1428, 1551, 2998, 3032, 3096, 3130
Channel B, Site B							
Fe^{2+}	1.948, 2.056, 2.163	1.905, 1.953	1.370/0.040	1.089−1.091	2.110, 2.217	116.6	1438, 1576, 2984, 3060, 3086
Co^{2+}	1.922, 2.032, 2.109	1.911, 1.933	1.363/0.033	1.089−1.092	2.148, 2.231	125.3	1451, 1590, 2963, 3056, 3076
Ni^{2+}	1.931, 1.979, 2.060	1.920, 1.920	1.362/0.032	1.089−1.092	2.159, 2.204	118.6	1462, 1599, 2977, 3063, 3085
Ni^{+}	1.927, 1.958	1.989, 2.109	1.397/0.067	1.087−1.091	1.987, 1.976	175.4	1454, 1538, 2972, 2997, 3051, 3089
Cu^{2+}	1.891, 2.009, 2.084	1.995, 2.107	1.384/0.054	1.086−1.088	1.988, 1.996	101.2	1445, 1556, 2984, 3006, 3120, 3149
Cu^{+}	1.924, 1.950	1.991, 2.095	1.389/0.059	1.085−1.088	1.966, 1.978	229.8	1443, 1548, 2987, 3013, 3123, 3150
Pd^{2+}	1.973, 2.131, 2.229	1.968, 2.215	1.374/0.044	1.083−1.091	2.208, 2.222	122.3	1458, 1572, 3005, 3103, 3123
Pd^{+}	2.186, 2.240	2.098, 2.522	1.382/0.052	1.084−1.089	2.145, 2.195	99.8	1449, 1555, 2996, 3033, 3083, 3132

[a] $\Delta R_{C=C}$: lengthening of the C=C bond upon adsorption, compared with free ethene molecule.

Table 4. Experimental[a] and Calculated Vibrational Frequencies of Ethene[b] in the Gas Phase

	harmonic frequencies	anharmonic frequencies	symmetry/ activity	mode[c]	exptl IR	exptl Raman
ν_1	3161	3024	A_g (R)	CH_2 s-str		3026
ν_2	1717	1682	A_g (R)	CC str		1623
ν_3	1389	1365	A_g (R)	CH_2 scis		1342
ν_4	1069	1047	A_u	CH_2 twist		
ν_5	3220	3074	B_{3g} (R)	CH_2 a-str		3103
ν_6	1241	1221	B_{3g} (R)	CH_2 rock		1236
ν_7	977	964	B_{3u} (IR)	CH_2 wag	949	
ν_8	962	948	B_{2g} (R)	CH_2 wag		943
ν_9	3246	3097	B_{2u} (IR)	CH_2 a-str	3106	
ν_{10}	832	830	B_{2u} (IR)	CH_2 rock	826	
ν_{11}	3145	2993	B_{1u} (IR)	CH_2 s-str	2989	
ν_{12}	1484	1449	B_{1u} (IR)	CH_2 scis	1444	

[a] Experimental data from ref 40. [b] B3LYP optimized bond lengths in ethene: C=C = 1.330 Å; C−H = 1.087 Å. [c] s, symmetric; a, asymmetric; str, stretching.

Ni^{2+} and Cu^{2+}, they are nearly equivalent. The monovalent cations Ni^{+} and Cu^{+} are coordinated to two framework atoms at both A2 and B sites; in their adsorption complexes, these bonds are lengthened. The Fe^{2+} and Co^{2+} cations from the A1a sites shift their position toward the adsorbate, and their coordination to the framework oxygen atoms undergoes change: two M−O bonds are slightly shortened and one is considerably lengthened. Divalent Ni^{2+} and Cu^{2+}, in contrast, undergo minor lengthening of the two shorter M−O bonds and considerable shortening of the third M−O bond. The divalent cations located in channel A form M−C bonds of lengths within 2.2−2.3 Å; only Pd^{2+} forms shorter M−C bonds. Pd^{+} at site A1a undergoes minor change in its coordination to the framework oxygen atoms upon adsorption. At B sites, all divalent cations lose coordination to one lattice oxygen atom when forming the adsorption complex, and the adsorption energies are higher than those for the A channel cations. It is worth noting that Ni^{+} cations at A2 sites and B sites have almost identical coordination to framework atoms and form adsorption complexes with similar geometry, and the vibrational frequencies appear very close. Thus, only diffraction methods would be able to distinguish Ni^{+} at these two sites.

Experimental data from microcalorimetry indicated adsorption energies of 80−100 kJ mol^{-1} for ethene adsorption in Cu(I)FAU and 55−65 kJ mol^{-1} for Cu(II)FAU,[10] but copper cations in FAU have their highest occupancy factors for sites SII inside the six-member rings, at which sites they form three shorter and three longer bonds to lattice oxygen atoms. It can be expected that adsorption energies for cation-exchanged clinoptilolite should be higher than those for FAU because clinoptilolite lacks six-member rings in which cations could be strongly confined and also because the adsorption energies of small hydrocarbons are known to increase with decreasing pore size.[42] Accordingly, the adsorption energies at cation sites in

dx.doi.org/10.1021/cs4005997 | ACS Catal. 2013, 3, 2759−2767

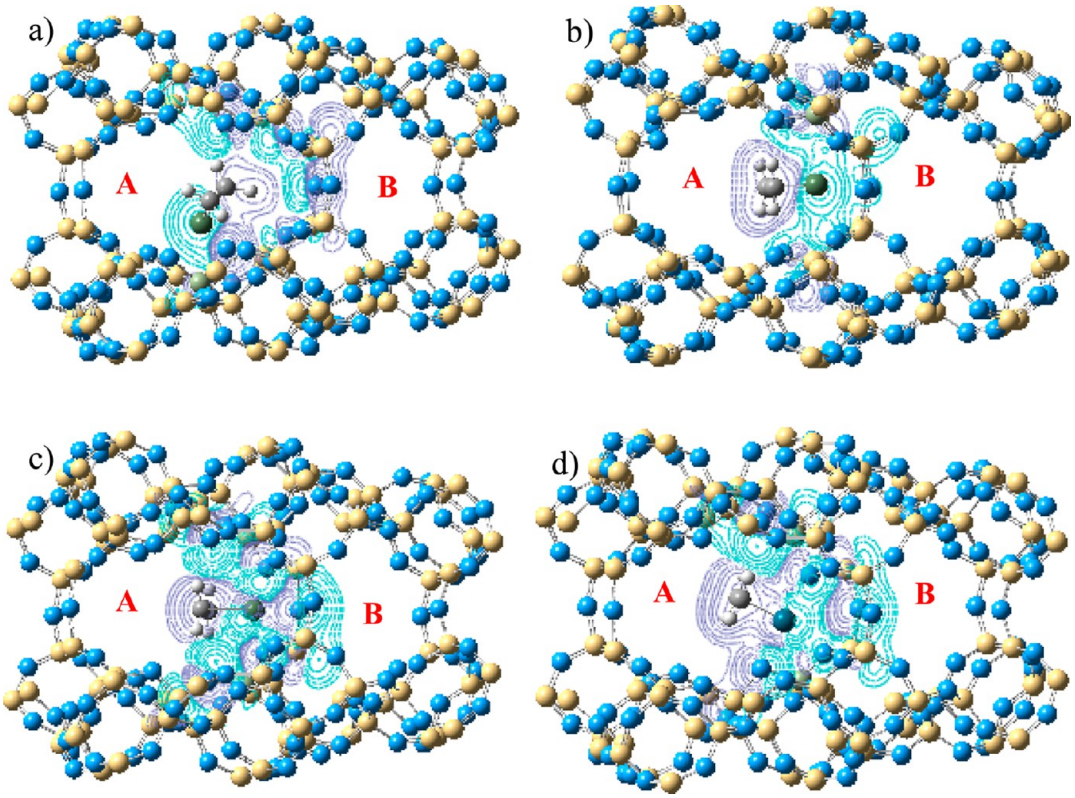

Figure 5. Deformation density contour plots describing the interactions between the zeolite framework and the adsorption complexes: (a) Zeo^{-}–$Ni(I)C_2H_4$ for Ni(I) at site A2, contour edges at ±0.001 au; (b) Zeo^{-}–$Ni(I)C_2H_4$ for Ni(I) at site A1, contour edges at ±0.001 au; (c) Zeo^{2-}–$Ni(II)C_2H_4$, with Ni(II) at site A1a, contour edges at ±0.002 au; (d) Zeo^{2-}–$Pd(II)C_2H_4$, with Pd(II) at site A1a, contour edges at ±0.002 au. The dark blue lines indicate regions with increased electron density; the light blue lines indicate depletion of electron density.

channel B are higher compared with those in channel A, with the exception of Ni^{+} and Cu^{+} cations at sites A2 and Pd cations (Pd^{2+}, Pd^{+}). DFT calculations of ethene adsorption complexes in Cu(I)MFI zeolites also indicated much higher adsorption energies of 175−194 kJ mol^{-1}.[14] The ethene molecule undergoes lengthening of the C═C bond upon adsorption, and this effect is very strong in the complexes formed in channel A with the monovalent cations Cu^{+} and Ni^{+} and with divalent Pd^{2+}.

The calculated frequency shift of the C═C vibrational mode is, on average, larger for adsorption in the A channel, 30−90 cm^{-1}, with a marked difference for monovalent cations and also Fe^{2+} and Pd^{2+}. The C−H bonds undergo significant changes in the adsorption complexes with Ni^{+} and Pd^{2+}, and the largest difference between the unequal C−H bonds is reached with Pd^{2+} at site B (0.008 Å), followed by Ni^{+} at sites A2 (0.006 Å). These results reveal activation of hydrogen atoms in the adsorbed ethene molecule, which depends not only on the cation type, but also on its location inside the zeolite. The CH_2 symmetric stretching vibrations undergo splitting, which is within 30 cm^{-1} for most adsorption complexes and larger only for Ni^{+} at the A2 sites (50 cm^{-1}). Lengthening of C−H bonds has been reported by theoretical studies of the reduction of light alkanes in transition-metal -exchanged ZSM-5, but not for alkenes.[43] The frequency shift of the C═C stretching vibration is not directly proportional to the C═C bond length change because the C−H bonds also experience the effect of π^* backdonation and the electrostatic potential within the clinoptilolite channels. Nevertheless, the frequency shift of the C═C vibration and the splitting of the corresponding band in the IR spectrum were considered as a possible way to discern olefin adsorption at different cation sites in FAU and ZSM-5, but the observed splitting for ethene was small, 10−12 cm^{-1}.[9]

The frequency shifts of the in-plane ring-stretching mode of benzene adsorbed in Cu(I)FAU and Cu(II)FAU were even smaller than those of ethene, and the benzene vibrational modes were not found to be related to the distinct cation sites in FAU.[45] According to our calculations, the frequency shifts cannot distinguish unambiguously the cations at B sites from those in channel A because they have similar coordination to framework oxygen atoms: asymmetric coordination to two or three oxygen atoms from the side rings. The adsorption complexes with Ni^{+} cations at sites A1 and A2 present more significant splitting of the C−H vibrations, which are detectable experimentally, but these effects cannot provide a simple rule to distinguish the different locations of the active sites.

The deformation density maps indicate the redistribution of electron density upon adsorption. The cations with largely filled d shells are able to donate electrons to the ethene molecule upon formation of the π-complex. The zeolite framework also plays a significant role, and the metal cations are "supplied" by electrons from the negatively charged framework. The number of framework oxygen atoms that donate electrons to the adsorption complex significantly exceeds the coordination number of the cations, and this applies to both the divalent and monovalent cations, as shown in Figure 5. Such an effect was not observed in studies of cation-exchanged MFI or FAU.[14] In channel A of clinoptilolite, the ethene molecule is exposed close to the center of the 10-member ring, and its orientation depends on the cation position. Thus, with Pd^{2+} cations at sites

dx.doi.org/10.1021/cs4005997 | ACS Catal. 2013, 3, 2759−2767

A1a, the adsorption complex approaches the center of channel A, but when Ni^+ resides at A1 sites, it remains closer to the channel wall. With divalent cations, the electron redistribution covers a broader area, and all oxygen atoms in the vicinity of the adsorption complex act as electron donors. The deformation density contour map patterns of Ni^{2+} and Pd^{2+} complexes have similar features, but monovalent Ni^+ at site A1 shows a pattern that is different from Ni^+ at site A2. The Ni^+ cations prefer site A2 among all available extraframework sites, which provides favorable disposition of the adsorption complex so that a larger number of framework oxygen atoms may contribute to the charge transfer. Ni^+ at site A1, being more confined to the narrow side of the 10-member rings, is able to attract electrons predominantly from the nearest coordinated oxygen atoms.

CONCLUSIONS

The adsorption of ethene at the divalent extraframework cations of the d elements (Fe^{2+}, Co^{2+}, Ni^{2+}, Cu^{2+}, Pd^{2+}) and at the monovalent cations Cu^+, Ni^+, and Pd^+ results in activation of both the C═C and C−H bonds. The C═C bond is lengthened most significantly upon adsorption at monovalent cations (Ni^+, Cu^+, Pd^+), whereas the C−H bonds are strongly activated in the adsorption complexes of Ni^+ and Pd^{2+}. The C−H bonds are affected in nonuniform way as they experience the electrostatic field in the channel. The activation of the C−H bonds results in splitting and shifting of the CH_2 symmetric stretching vibrations of ethene adsorbed in clinoptilolite, which are detectable experimentally (splitting and shifting of the 3024 cm^{-1} frequency band), but these effects are smaller than the frequency shift related to the weakening of the C═C bond. The frequency shift of the C═C vibration differs by 25−35 cm^{-1} for the adsorption complexes in A and B channel with Fe^{2+} and Pd^{2+} cations, but for the other cations, the differences are smaller. The analysis of deformation density indicates a charge-transfer component from the metal cations to ethene, and the framework oxygen atoms also contribute by donating electrons to the cations. The clinoptilolite 10-member rings of channel A provide a second coordination sphere to the adsorption complex because more than the nearest to the cations oxygen atoms participate in electron donation. On the basis of the site preference of the divalent cations to the large channel A in dehydrated clinoptilolite, it can be suggested that ethene adsorption complexes would form primarily in this channel. The calculated adsorption energies of ethene in clinoptilolite are high because the cations are only side-on-coordinated to the framework oxygen atoms and exposed as nearly bare adsorption centers.

ASSOCIATED CONTENT

Supporting Information

Table S1 with ONIOM calculated bond lengths and angles in proximity of the cation sites in clinoptilolite, figures with cation site locations for the different extraframework cations, and optimized geometries for different Si/Al ratio (15 pages). This information is available free of charge via the Internet at http://pubs.acs.org.

AUTHOR INFORMATION

Corresponding Author

*E-mail: ellie@svr.igic.bas.bg.

Notes

The authors declare no competing financial interest.

ACKNOWLEDGMENTS

The computational results presented have been achieved in part using the Vienna Scientific Cluster (VSC). E.L.U. acknowledges CPU time at the high-performance cluster MADARA of the Bulgarian Academy of Sciences.

REFERENCES

(1) Davis, M. E. *Ind. Eng. Chem. Res.* **1991**, *30*, 1675−1683. Davis, M. E. *Acc. Chem. Res.* **1993**, *26*, 111−115.
(2) Yang, R. T. *Gas Separation by Adsorption Processes*; Butterworth: Boston, 1987.
(3) Palomino, G. T.; Bordiga, S.; Zecchina, A.; Marra, G. L.; Lamberti, C. *J. Phys. Chem. B* **2000**, *104*, 8641−8651.
(4) (a) Rice, M.; Chakraborty, A. K.; Bell, A. T. *J. Phys. Chem. B* **2000**, *104*, 9987−9992. (b) Bao, X.; Sung, C.-Y.; Snurr, R. Q.; Broadbelt, L. *ACS Catal.* **2012**, *2*, 350−359.
(5) Kuroda, Y.; Iwamoto, M. *Top. Catal.* **2004**, *28*, 111−118.
(6) (a) Choi, E. Y.; Kim, S. Y.; Kim, Y.; Seff, K. *Microporous Mesoporous Mater.* **2003**, *62*, 201−210. (b) Zhen, S.; Seff, K. *Microporous Mesoporous Mater.* **2000**, *39*, 1−18. (c) Jang, S. B.; Jeong, M. S.; Kim, Y.; Seff, K. *J. Phys. Chem. B* **1997**, *101*, 9041−9045. (d) Lee, Y. M.; Choi, S. J.; Kim, Y.; Seff, K. *J. Phys. Chem. B* **2005**, *109*, 20137−20144.
(7) Hübner, G.; Rauhut, G.; Stoll, H.; Roduner, E. *Phys. Chem. Chem. Phys.* **2002**, *4* (13), 3112−3121.
(8) Hübner, G.; Rauhut, G.; Stoll, H.; Roduner, E. *J. Phys. Chem. B* **2003**, *107*, 8568−8573.
(9) Datka, J.; Kukulska-Zając, E. *J. Phys. Chem. B* **2004**, *108*, 17760−17766.
(10) Borgard, G. D.; Molvik, S.; Balaraman, P.; Root, T. W.; Dumesic, J. A. *Langmuir* **1995**, *11*, 2065−2070.
(11) (a) Yang, R. T.; Kikkinides, E. S. *AIChE J.* **1995**, *41*, 509−517. (b) Chen, N.; Yang, R. T. *Ind. Eng. Chem. Res.* **1996**, *35*, 4020−4027.
(12) Padin, J.; Yang, R. T. *Chem. Eng. Sci.* **2000**, *55* (14), 2607−2616.
(13) Godelitsas, A.; Charistos, D.; Tsipis, A.; Tsipis, C.; Filippidis, A.; Triantafyllidis, C.; Manos, G.; Siapkas, D. *Chem.—Eur. J.* **2001**, *7*, 3705−3721.
(14) Rejmak, P.; Mitoraj, M.; Broclawik, E. *Phys. Chem. Chem. Phys.* **2010**, *12*, 2321−2330.
(15) (a) Hartmann, M.; Kevan, L. *J. Chem. Soc., Faraday Trans.* **1996**, *92*, 1429−1434. (b) Hartmann, M.; Kevan, L. *Chem. Rev.* **1999**, *99* (3), 635−664.
(16) (a) Choo, H.; Kevan, L. *J. Phys. Chem. B* **2001**, *105*, 6353−6360. (b) Choo, H.; Hong, S. B.; Kevan, L. *J. Phys. Chem. B* **2001**, *105*, 7730−7738. (c) Choo, H.; Prakash, A. M.; Park, S. K.; Kevan, L. *J. Phys. Chem. B* **1999**, *103*, 6193−6199.
(17) Misaelides, P. *Microporous Mesoporous Mater.* **2011**, *144*, 15−18.
(18) Khodabandeh, S.; Davis, M. E. *Microporous Mater.* **1997**, *9*, 149−160.
(19) Godelitsas, Ath.; Armbruster, Th. *Microporous Mesoporous Mater.* **2003**, *61*, 3−24.
(20) Garcia-Basabe, Y.; Ruiz-Salvador, A.; Maurin, G.; de Menorval, L.-C.; Rodriguez-Iznaga, I.; Gomez, A. *Microporous Mesoporous Mater.* **2012**, *155*, 233−239.
(21) Schoonheydt, R. A.; Weckhuysen, B. A. *Phys. Chem. Chem. Phys.* **2009**, *11*, 2794−2798.
(22) Baerlocher, Ch.; McCusker, L. B.; Olson, D. H. *Atlas of Zeolite Framework Types*, 6th rev. ed.; Elsevier: Amsterdam, 2007.
(23) Alberti, A. *Tschermaks Mineral. Petrogr. Mitt.* **1975**, *22*, 25−37.
(24) Koyama, K.; Takéuchi, Y. *Z. Kristallogr.* **1977**, *145*, 216−239.
(25) Dapprich, S.; Komáromi, I.; Byun, K. S.; Morokuma, K.; Frisch, M. J. *J. Mol. Struct.: THEOCHEM* **1999**, *462*, 1−21.
(26) (a) Vreven, T.; Byun, K. S.; Komáromi, I.; Dapprich, S.; Montgomery, J. A., Jr.; Morokuma, K.; Frisch, M. J. *J. Chem. Theory and Comput.* **2006**, *2*, 815−826. (b) Vreven, T.; Frisch, M. J.; Kudin, K. N.; Schlegel, H. B.; Morokuma, K. *Mol. Phys.* **2006**, *104*, 701−714. (c) Fermann, J. T.; Moniz, T.; Kiowski, O.; McIntire, T. J.; Auerbach, S. M.; Vreven, T.; Frisch, M. J. *J. Chem. Theory Comput.* **2005**, *1*,

1232−1239. (d) Clemente, F.; Vreven, T.; Frisch, M. J. In *Quantum Biochemistry*; Matta, C., Ed.; Wiley VCH: Weinheim, 2010.
(27) Frisch, M. J.; Trucks, G. W.; Schlegel, H. B.; Scuseria, G. E.; Robb, M. A.; Cheeseman, J. R.; Scalmani, G.; Barone, V.; Mennucci, B.; Petersson, G. A.; Nakatsuji, H.; Caricato, M.; Li, X.; Hratchian, H. P.; Izmaylov, A. F.; Bloino, J.; Zheng, G.; Sonnenberg, J. L.; Hada, M.; Ehara, M.; Toyota, K.; Fukuda, R.; Hasegawa, J.; Ishida, M.; Nakajima, T.; Honda, Y.; Kitao, O.; Nakai, H.; Vreven, T.; Montgomery, J. A., Jr.; Peralta, J. E.; Ogliaro, F.; Bearpark, M.; Heyd, J. J.; Brothers, E.; Kudin, K. N.; Staroverov, V. N.; Kobayashi, R.; Normand, J.; Raghavachari, K.; Rendell, A.; Burant, J. C.; Iyengar, S. S.; Tomasi, J.; Cossi, M.; Rega, N.; Millam, N. J.; Klene, M.; Knox, J. E.; Cross, J. B.; Bakken, V.; Adamo, C.; Jaramillo, J.; Gomperts, R.; Stratmann, R. E.; Yazyev, O.; Austin, A. J.; Cammi, R.; Pomelli, C.; Ochterski, J. W.; Martin, R. L.; Morokuma, K.; Zakrzewski, V. G.; Voth, G. A.; Salvador, P.; Dannenberg, J. J.; Dapprich, S.; Daniels, A. D.; Farkas, Ö.; Foresman, J. B.; Ortiz, J. V.; Cioslowski, J.; Fox, D. J. *Gaussian 09, Revision D.01*; Gaussian, Inc.: Wallingford CT, 2009.
(28) Grigoras, S.; Lane, T. H. *J. Comput. Chem.* **1987**, *8*, 84−93.
(29) (a) Perdew, J. P.; Burke, K.; Ernzerhof, M. *Phys. Rev. Lett.* **1996**, *77*, 3865−3868. (b) Perdew, J. P.; Burke, K.; Ernzerhof, M. *Phys. Rev. Lett.* **1997**, *78*, 1396.
(30) Lee, C.; Yang, W.; Parr, R. G. *Phys. Rev.* **1988**, *B37*, 785−789.
(31) Miehlich, B.; Savin, A.; Stoll, H.; Preuss, H. *Chem. Phys. Lett.* **1989**, *157*, 200−206.
(32) Becke, A. D. *J. Chem. Phys.* **1993**, *98*, 5648−5652.
(33) (a) Wachters, A. J. H. *J. Chem. Phys.* **1970**, *52*, 1033. (b) Hay, P. J. *J. Chem. Phys.* **1977**, *66*, 4377−4384. (c) Raghavachari, K.; Trucks, G. W. *J. Chem. Phys.* **1989**, *91*, 1062−1065. (d) Hay, P. J.; Wadt, W. R. *J. Chem. Phys.* **1985**, *82*, 270−283.
(34) Weigend, F.; Ahlrichs, R. *Phys. Chem. Chem. Phys.* **2005**, *7*, 3297−3305.
(35) Andrae, D.; Häussermann, U.; Dolg, M.; Stoll, H.; Preuss, H. *Theor. Chim. Acta* **1990**, *77*, 123−141.
(36) Rappé, A. K.; Casewit, C. J.; Colwell, K. S.; Goddard, W. A., III; Skiff, W. M. *J. Am. Chem. Soc.* **1992**, *114*, 10024−10035.
(37) (a) Barone, V.; Minichino, C. *J. Mol. Struct.: THEOCHEM* **1995**, *330*, 365−376. (b) Barone, V. *J. Chem. Phys.* **2004**, *120*, 3059−3065. (c) Barone, V. *J. Chem. Phys.* **2005**, *122* (014108), 1−10.
(38) (a) Uzunova, E. L.; Mikosch, H. *J. Phys. Chem. B* **2004**, *108*, 6981−6987. (b) Uzunova, E. L.; Mikosch, H. *J. Mol. Struct.: THEOCHEM* **2009**, *912*, 88−94. (c) Uzunova, E. L.; Mikosch, H.; Nikolov, G. St. *Int. J. Quantum Chem.* **2013**, *113*, 723−728. (d) Uzunova, E. L.; Mikosch, H. *Microporous Mesoporous Mater.* **2013**, *177*, 113−119.
(39) Johnson, M.; O'Connor, D.; Barnes, P.; Catlow, C. R. A.; Owens, S. L.; Sankar, G.; Bell, R.; Teat, S. J.; Stephenson, R. *J. Phys. Chem. B* **2003**, *107*, 942−951.
(40) Shimanouchi, T. *Tables of Molecular Vibrational Frequencies Consolidated*; National Bureau of Standards: Washington, D.C., 1972; Vol. *I*.
(41) Ogihara, S.; Iijima, A. *Eur. J. Mineral.* **1990**, *2*, 819−826.
(42) (a) Derouane, E. G.; André, J.-M.; Lucas, A. A. *J. Catal.* **1988**, *110*, 58−73. (b) Derouane, E. G.; Leherte, L.; Vercauteren, D. P.; Lucas, A. A.; André, J.-M. *J. Catal.* **1989**, *119*, 266−268.
(43) (a) Pidko, E. A.; van Santen, R. A. *J. Phys. Chem. C* **2007**, *111*, 2643−2655. (b) Pidko, E. A.; Hensen, E. J. M.; van Santen, R. A. *J. Phys. Chem. C* **2007**, *111*, 13068−13075.
(44) Armbruster, T.; Simoncic, P.; Döbelin, N.; Malsy, A.; Yang, P. *Microporous Mesoporous Mater.* **2003**, *57*, 121−131.
(45) Archipov, T.; Santra, S.; Ene, A. B.; Stoll, H.; Rauhut, G.; Roduner, E. *J. Phys. Chem. C* **2009**, *113*, 4107−4116.